Stoichiometric formation of an oxoiron(IV) complex by a soluble methane monooxygenase type activation of O_2 at an iron(II)-cyclam centre

Dustin Kass,[‖] Teresa Corona,[‖] Katrin Warm,[‖] Beatrice Braun-Cula,[‖] Uwe Kuhlmann,[⌜] Eckhard Bill,[⊥] Stefan Mebs,[†] Marcel Swart,[Ψ] Holger Dau,[†] Michael Haumann,[†] Peter Hildebrandt,[⌜] Kallol Ray[‖,*]

[‖]Institut für Chemie, Humboldt-Universität zu Berlin, Brook-Taylor-Straße 2, 12489 Berlin, Germany; [⊥]Max-Planck-Institut für Chemische Energiekonversion, Stiftstrasse 34 – 36, 45470 Mülheim an der Ruhr, Germany; [⌜] Department of Chemistry, Technische Universität Berlin, Straße des 17. Juni 135, 10623 Berlin, Germany; [†] Department of Physics, Freie Universität Berlin, Arminallee 14, 14195 Berlin, Germany; [Ψ]ICREA Pg. Lluis Companys 23, 08010 Barcelona, Spain; and IQCC,Universitat de Girona, Campus Montilivi 17003 Girona, Spain.

Supporting Information Placeholder

ABSTRACT: In soluble methane monooxygenase enzymes (*s*MMO) dioxygen (O_2) is activated at a diiron(II) center to form an oxodiiron(IV) intermediate **Q** that performs the challenging oxidation of methane to methanol. An analogous mechanism of O_2 activation at mono- or di-nuclear iron centres is rare in the synthetic chemistry. Herein, we report a mononuclear non-heme iron(II)-cyclam complex **1**-*trans* that activates O_2 to form the corresponding iron(IV)-oxo complex **2**-*trans* *via* a mechanism reminiscent of the O_2 activation process in *s*MMO. The conversion of **1**-*trans* to **2**-*trans* proceeds *via* the intermediate formation of an iron(III)-superoxide species **3**, which could be trapped and spectroscopically characterized at –50°C. Surprisingly, **3** is a stronger oxygen atom transfer (OAT) agent than **2**-*trans*; **3** performs OAT to **1**-*trans* or PPh_3 to yield **2**-*trans* quantitatively. Furthermore, **2**-*trans* oxidizes the aromatic C-H bonds of 2,6-di-*tert*-butylphenol, which, together with the strong OAT ability of **3** represent new domains of oxoiron(IV) and superoxoiron(III) reactivities.

High-valent oxoiron(IV) and formally oxoiron(V) species act as active intermediates in the catalytic cycles of a number of enzymatic systems.[1-12] Heme and non-heme proteins generate these reactive intermediates to couple the activation of dioxygen to the oxidation of their substrates.[13-23] O_2 activation generally occurs at an iron(II) center to form an iron(III)–superoxo intermediate, which converts the kinetically inert ground state of O_2 to a more reactive doublet state of superoxide ($O_2^{\bullet-}$). In mononuclear enzymes, the generated iron(III)–superoxo species picks up an electron and a proton to form an iron(III)–hydroperoxo intermediate, which then undergoes O–O bond cleavage to afford the reactive high-valent iron–oxo species responsible for substrate oxidation reactions.[16-18] In dinuclear enzymes, on the other hand, direct activation of O_2 occurs at a diiron(II) centre to form either closed bis(μ-oxo)diiron(IV) or open $O{=}Fe^{IV}$-O-$Fe^{IV}{=}O$ forms, without the necessity of any additional proton or electron donors.[18-22]

In biomimetic chemistry, the generation of iron-oxo species has recently been demonstrated by activation of O_2 at non-heme iron(II) model complexes in the presence of electron and proton donors.[24-27] We now show a novel bimolecular activation of dioxygen at a model iron(II) center to generate an oxoiron(IV) species, reminiscent of the proposed O_2 activation mechanism in methane monooxygenase (*s*MMO; Scheme 1 and Scheme 2).

Scheme 1. Overview of the formation of 2-*cis* and 2-*trans* from their corresponding iron(II) *cyclam* isomers 1-*cis* and 1-*trans*.

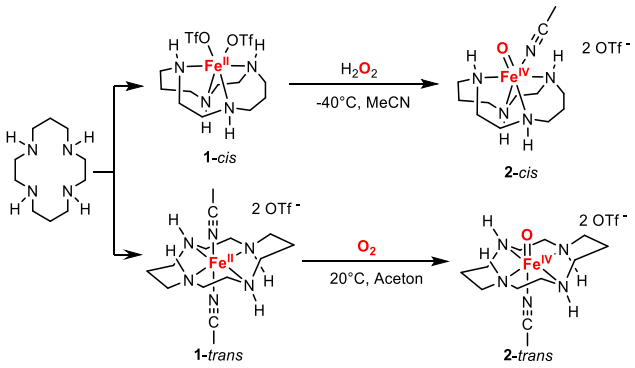

As previously reported,[28] combination of the tetradentate cyclam ligand with $[Fe(OTf)_2(CH_3CN)_2]$ (OTf=$CF_3SO_3^-$) yields the iron(II) cyclam complex, $[(cyclam)Fe^{II}(OTf)_2]$ (**1**-*cis*), in *cis*-V configuration of the macrocyclic ring and two *cis* triflates.[29-30] In contrast, in solution, CH_3CN gradually replaces the bound triflate ligands of **1**-*cis* to form $[(cyclam)Fe^{II}(CH_3CN)_2]$ (**1**-*trans*) (over a period of 24 hours at 25 °C in the absence of O_2) with a concomitant change to the *trans*-III configuration with two *trans*-CH_3CN ligands (Figure S1).[29] The zero-field Mössbauer spectrum (Figure S2) of solid **1**-*trans* at 14 K reveals a single quadrupole doublet with an isomer shift δ of 0.53 mm s^{-1} and a small quadrupole splitting (ΔE_Q) of 0.61 mm s^{-1}, demonstrating that the iron(II) center remains in the low-spin configuration (S = 0).[31] The diamagnetic ground state of **1**-*trans* is maintained in CH_3CN solution, as evident from ^{1}H-NMR studies (Figure S3), which reveal peaks between 1.5 – 3.7 ppm. **1**-*cis*, in contrast, displays paramagnetically shifted ^{1}H-NMR signals between –10 – 130 ppm (Figure S4). Furthermore, zero-field Mössbauer measurements on solid **1**-*cis* confirmed its

high-spin $S = 2$ ground state with $\delta = 1.15$ mm s^{-1} and $\Delta E_Q = 2.31$ mm s^{-1} (Figure S5).

The different spin states of the iron(II) centers in **1**-*cis* and **1**-*trans* are reflected in their reactivity properties. As reported in our previous study,[28] **1**-*cis* reacts with H_2O_2 to generate [(cyclam)Fe^{IV}(O)(CH$_3$CN)]$^{2+}$ (**2**-*cis*) (Figure S6) as a kinetically and catalytically competent intermediate to perform the epoxidation of olefins with high stereo- and regioselectivity. For **1**-*trans*, in contrast, no catalytic epoxidation reactions in presence of H_2O_2 are observed.

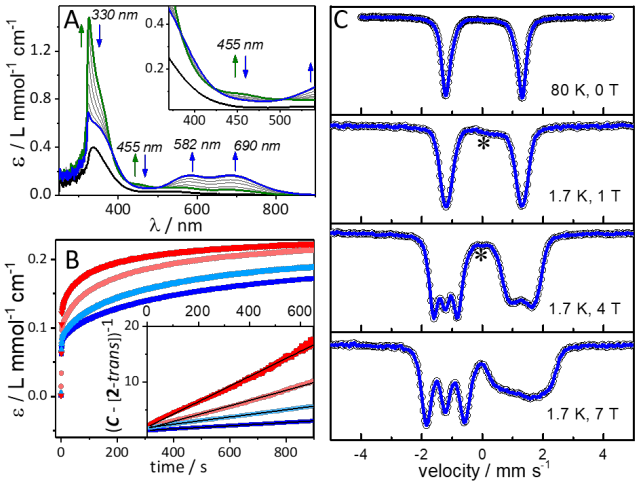

Figure 1 A) UV-vis spectral changes associated with the initial conversion of **1**-*trans* (black) upon addition of O_2 to **3** (green) followed by the formation of **2**-*trans* (blue) in acetone at –20 °C; B) time traces of the development of the 690 nm band of **2**-*trans* in presence of pure O_2 (blue), 75/25 (light blue) O_2/N_2 mixture, 50/50 (light red) O_2/N_2 mixture and air (red); the inset shows the plot of the inverse *C*-[**2**-*trans*] (*C* = initial concentration of **1**-*trans*) against time and the corresponding linear fits proving second order behavior (black); C) Mössbauer spectra of ^{57}Fe-enriched **2**-*trans* (2 mM, frozen acetone solution) recorded at 1.7 and 80 K and different magnetic fields and the corresponding simulation based on an intermediate spin (S = 1) iron(IV) species (blue; 96%) ($\delta = 0.05$ mm/s, $\Delta E_Q = +2.49$ mm/s, $\eta = 0$, $A_{xx} = -23.1$, $A_{yy} = -23.1$, $A_{zz} = -2.6$ /$g_N\beta_N$ Tesla; D = 25 cm^{-1}). The symbol "*" represents minor contributions from S = 0 Fe^{II} impurities. For complete simulation see Figure S11 B.

1-*trans* is air stable in CH$_3$CN at 25 °C. However, bubbling of O_2 or air at –20 ^{0}C to an acetone solution[32] of **1**-*trans* (Figure S7) leads to the immediate formation of an intermediate **3** with absorption maxima λ_{max} (ϵ_{max}) centered at 330 nm (1800 M^{-1}cm^{-1}) and 455 nm (116 M^{-1}cm^{-1}) (green trace Figure 1A and S8) which then converts to a stable blue species **2**-*trans* ($t_{1/2}$ =120 min at 25 °C; paramagnetic shifted ^{1}H-NMR is shown in Figure S9), with two characteristic absorption bands of equal intensities at 583 and 690 nm (ε_{max}=198 M^{-1}cm^{-1}; Figure 1A blue trace). Single crystals of **2**-*trans* were grown from acetone/diethyl ether at –40°C, and a crystallographic analysis shows **2**-*trans* as a structural isomer of **2**-*cis*, with a terminal Fe=O moiety and a *trans*-III (instead of *cis*-V in **2**-*cis*) configuration of the macrocyclic ring (Figure 2B; Tables S1-S2). Further characterizations of **2**-*trans*, were performed by a variety of spectroscopic methods (Figure S9-S13). The zero-field Mössbauer spectrum of **2**-*trans* (Figure 1C; $\Delta E_Q = 2.49$ mm s^{-1}, $\delta = 0.05$ mm s^{-1}) is consistent with the presence of an Fe^{IV} center. Furthermore, in presence of applied field (Figure 1C and Figure S11B), the observed hyperfine structures and specifically the field dependence can be well simulated with $S = 1$ Hamiltonian and zero-field splitting and magnetic hyperfine tensors that are typical of $S = 1$ Fe^{IV} centers.[1-4,33] The resonance Raman (RR) spectrum (Figure 2A) obtained with λ_{ex} = 413 nm exhibits a band at 842 cm^{-1} which upon ^{18}O-labelling is replaced by two new peaks at 800 and 813 cm^{-1} originating from a Fermi doublet (ν^0 = 806 cm^{-1}).[34-35] Analysis of the extended X-ray absorption fine structure (EXAFS) of **2**-*trans* in acetone solution (Figure S12, Table S1) yields the best fit comprising an oxygen ligand at 1.67 Å, which is assigned to an Fe=O unit, as well as 4 O/N and 1 O/N ligands at 2.00 Å and 2.10 Å, respectively, which correspond to the N donors of the cyclam and CH$_3$CN ligands. The Fe *K*-edge X-ray absorption spectrum of **2**-*trans* (Figure S13) reveals a pronounced pre-edge amplitude at ca. 7114.8 eV and a K-edge energy of 7123.9 eV, which are typical of Fe^{IV}=O complexes.[36] DFT calculations on **2**-*trans* (Table S3) predict an $S = 1$ ground-state with calculated Fe=O bond-distance (1.64 Å), stretching mode frequency (867 cm^{-1}, ^{18}O isotope shift -35 cm^{-1}) and Mössbauer δ-value (0.02 mm s^{-1}) in good agreement with experiments.

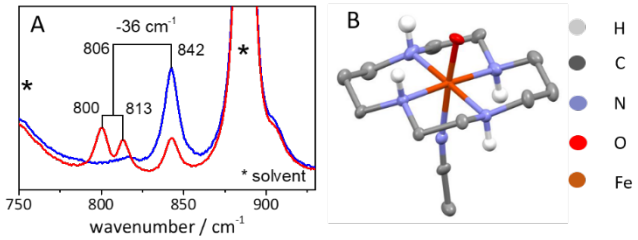

Figure 2 A) Normalized RR spectra of **2**-*trans* (blue) and ^{18}O-enriched **2**-*trans* (red) (λ_{ex} = 413 nm, T= –30 °C in acetone) B) The crystal structure of **2**-*trans* (CH$_2$- and CH$_3$- hydrogens and two triflate counterinions are omitted for clarity) .

The transient intermediate **3** at –20 °C could be trapped by lowering of the temperature to –50 °C. The Mössbauer spectrum of **3** recorded at 2 K with a magnetic field of 1T exhibits a doublet representing about 86 % of the iron with $\Delta E_Q = -2.85$ mm s^{-1} and $\delta = 0.27$ mm s^{-1} (Figure S14), which is consistent with a low-spin iron(III) assignment. Further applied field measurements (Figure S14) determine the negative sign of the electric field gradient and confirm an $S = 0$ assignment, arising from an antiferromagnetic coupling of the $S = 1/2$ Fe^{III} center with the $S = 1/2$ superoxide ($O_2^{-\bullet}$) radical. Consistent with the superoxide assignment,[9, 37] the RR spectrum (Figure S15) of a 1 mM solution of **3** in acetone at –90 °C exhibits a ν(O-O) stretch at 1147 cm^{-1}, which upon ^{18}O-labelling is presumably shifted to the 1050–1100 cm^{-1} region, where it is obscured by the intense solvent signals (CH$_3$COCH$_3$ or CD$_3$COCD$_3$). XAS revealed an Fe *K*-edge energy of **3** in between the energies of **1**-*trans* and **2**-*trans* (Figure S13), supporting the Fe(III) assignment of **3**, as well as a relatively short Fe-O bond of ~1.74 Å from EXAFS (Figure S12, Table S1). DFT calculations in the $S = 0$ ground state support an end-on binding mode of $O_2^{-\bullet}$ in **3**, with a calculated ν(O-O) vibration at 1167 cm^{-1}, and Mössbauer data of ΔE_Q= –2.59 mm s^{-1} and δ=0.18 mm s^{-1}, and an Fe-O bond of 1.76 Å, in good agreement with the experiments (Tables S1, S3).

The kinetics of the oxygen uptake process during the conversion of **1**-*trans* to **2**-*trans* were monitored spectrophotometrically by measuring the increase of the absorbance of the oxoiron(IV) complex at 690 nm at –20 °C. It shows a second-order behavior for the formation of **2**-*trans*, as evident from the observed linear correlation in the inverse *C*–[**2**-*trans*] *vs* time plot (Figure 1B inset, equation S6; *C* is the initial concentration of **1**-*trans*). In O_2, the observed second-order rate constant k_{obs} is 2.6 M^{-1} s^{-1}. Interestingly, the reaction performed under air is much faster (Figure 1B), with a

corresponding rate constant of 22.6 M^{-1} s^{-1}. Reactions with different O_2/N_2 mixtures (O_2/N_2 75/25 k_{obs} 5.9 M^{-1} s^{-1}, 50/50 k_{obs}=12.6 M^{-1} s^{-1}) (Figure 1B, inset and Figure S16) further confirmed an inverse first-order dependence of the reaction rate on O_2 (equations S4 and S5). Notably, the use of deuterated acetone or the d_4-**2**-*trans* complex (where the –NH groups of the cyclam ligand are deuterated) revealed no difference in reaction rates (Figure S17), excluding the involvement of the solvent or the cyclam N–H groups as proton or electron donors in the reaction of **1**-*trans* with O_2 to form **2**-*trans*.

The observed rate law (equations S3 and S4) is consistent with a reaction mechanism involving strong complexation of O_2 by one molecule of **1**-*trans* to form **3**. A preequilibrium release of O_2 from **3** regenerates **1**-*trans* in minor quantities; residual **3** then transfers an oxygen atom to the *in situ* generated **1**-*trans* to yield two molecules of **2**-*trans* (Scheme 2A). Under these conditions a buildup of **1**-*trans* is avoided in the reaction mixture, which would otherwise lead to the bimolecular decay of **2**-*trans* to form Fe^{III}-O-Fe^{III} as the thermodynamic sink. Indeed, addition of **1**-*trans* to **3** at −50 °C does not lead to the formation of **2**-*trans*. However, fast oxygen atom transfer (OAT) from **3** to PPh_3 is observed at −50 °C leading to the quantitative formation of **2**-*trans* and PPh_3O (Figure S18).

Scheme 2. A) Proposed reaction mechanism of the formation of 2-*trans* in the reaction of 1-*trans* with O_2 B) The corresponding mechanism for O_2 activation at the diiron active site in *s*MMO (B) [4, 19-20].

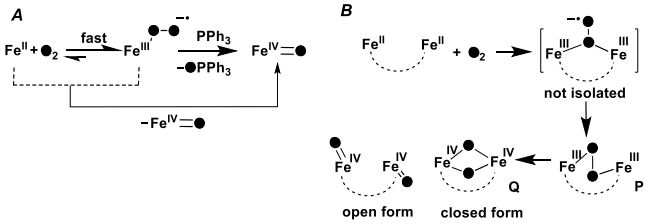

2-*trans* is a sluggish oxidant and does not react with PPh_3 at −50 °C. Thus, it is a weaker OAT agent relative to **3**. At 25 °C **2**-*trans* performs OAT to PPh_3 and hydrogen atom abstraction (HAA) from dihydroanthracene, xanthene, cyclohexadiene, and fluorene at rates that are 2-3 orders of magnitude slower than for **2**-*cis* (Table S4; Figure S19). A significantly larger ^{2}H-kinetic isotope effect of 20 has been determined for xanthene oxidation by **2**-*trans* (Figure S20) in contrast to the value of 6.7 previously reported for **2**-*cis*.[28] Furthermore, **2**-*trans* demonstrates a unique ability to oxidize the aromatic C-H bonds in phenols (Scheme S1); for example the reaction with 2,6-di-*tert*-butyl-phenol (DTBP) led to the formation of 2,6-di-*tert*-butyl-1,4-benzoquinone (DTQ) and the C-C coupled dimer 2,2′,6,6′-tetra-*tert*-butyl-1,1′-biphenol (DTP) in 32% and 23% yields, respectively. Isotope labelling studies confirmed that one of the oxygen atoms in DTQ is derived from the Fe^{IV}=O moiety in **2**-*trans* (Figures S26-S27). Although analogous conversion of DTBP to DTQ mediated by metal-superoxo complexes [38-39] is reported, this is unprecedented in oxoiron(IV) chemistry.

In summary, a non-heme iron(II) complex **1**-*trans* reacts rapidly with dioxygen to form an oxoiron(IV) complex **2**-*trans* via an unprecedented mechanism that is second order in iron and inverse first order in O_2. An iron(III)-superoxide species has been identified as an intermediate in the reaction, which is found to be a stronger OAT agent than **2**-*trans*. The present results are relevant to the chemistry of dinuclear non-heme iron enzymes (Scheme 2B) like *s*MMO that catalyze the conversion of CH_4 to CH_3OH, one of the most difficult chemical oxidations, *via* dioxygen activation. The O_2 activation ability is unique for **1**-*trans* with a *trans*-III configuration of the cyclam macrocyclic ring and two *trans*-axial ligands. Future studies, including theoretical calculations, will focus on obtaining further insights into the specific reactivity properties of **1**-*trans* and **2**-*trans*.

ASSOCIATED CONTENT

Supporting Information

The Supporting Information is available free of charge at:

Instrumental and physical methods, synthesis of compounds and intermediates, reactivity studies, theoretical studies and additional Figures S1-S27 (further characterization and reactivity data) and Tables S1-S4 (crystallography, EXAFS and DFT data).

AUTHOR INFORMATION

Corresponding Author

Kallol.Ray@chemie.hu-berlin.de

Notes

The authors declare no competing financial interest.

ACKNOWLEDGMENT

This work was funded by the Deutsche Forschungsgemeinschaft (EXC 314-2 and EXC 2008/1 to K.R., P.H. and H.D. and the Heisenberg-Professorship to K.R.), Alexander von Humboldt Foundation to TC, MINECO (CTQ2017-87392-P) and FEDER (UNGI10-4E-801) to MS. We thank Dr. Christian Herwig for the preparation of different O_2/N_2 mixtures.

REFERENCES

1. Rohde, J.-U.; Stubna, A.; Bominaar, E. L.; Münck, E.; Nam, W.; Que, L., Nonheme Oxoiron(IV) Complexes of Tris(2-pyridylmethyl)amine with cis-Monoanionic Ligands. *Inorganic Chemistry* **2006,** *45* (16), 6435-6445.
2. Hohenberger, J.; Ray, K.; Meyer, K., The biology and chemistry of high-valent iron–oxo and iron–nitrido complexes. *Nature Communications* **2012,** *3* (1), 720.
3. Nam, W.; Lee, Y.-M.; Fukuzumi, S., Tuning Reactivity and Mechanism in Oxidation Reactions by Mononuclear Nonheme Iron(IV)-Oxo Complexes. *Accounts of Chemical Research* **2014,** *47* (4), 1146-1154.
4. Ray, K.; Pfaff, F. F.; Wang, B.; Nam, W., Status of Reactive Non-Heme Metal–Oxygen Intermediates in Chemical and Enzymatic Reactions. *Journal of the American Chemical Society* **2014,** *136* (40), 13942-13958.
5. Cook, S. A.; Borovik, A. S., Molecular Designs for Controlling the Local Environments around Metal Ions. *Accounts of Chemical Research* **2015,** *48* (8), 2407-2414.
6. Puri, M.; Que, L., Toward the Synthesis of More Reactive S = 2 Non-Heme Oxoiron(IV) Complexes. *Accounts of Chemical Research* **2015,** *48* (8), 2443-2452.
7. Ray, K.; Heims, F.; Schwalbe, M.; Nam, W., High-valent metal-oxo intermediates in energy demanding processes: from dioxygen reduction to water splitting. *Current Opinion in Chemical Biology* **2015,** *25*, 159-171.
8. Engelmann, X.; Monte-Pérez, I.; Ray, K., Oxidation Reactions with Bioinspired Mononuclear Non-Heme Metal–Oxo Complexes. *Angewandte Chemie International Edition* **2016,** *55* (27), 7632-7649.

9. Baglia, R. A.; Zaragoza, J. P. T.; Goldberg, D. P., Biomimetic Reactivity of Oxygen-Derived Manganese and Iron Porphyrinoid Complexes. *Chemical Reviews* **2017,** *117* (21), 13320-13352.
10. Huang, X.; Groves, J. T., Oxygen Activation and Radical Transformations in Heme Proteins and Metalloporphyrins. *Chemical Reviews* **2018,** *118* (5), 2491-2553.
11. Guo, M.; Corona, T.; Ray, K.; Nam, W., Heme and Nonheme High-Valent Iron and Manganese Oxo Cores in Biological and Abiological Oxidation Reactions. *ACS Cent Sci* **2019,** *5* (1), 13-28.
12. Chen, Z.; Yin, G., The reactivity of the active metal oxo and hydroxo intermediates and their implications in oxidations. *Chemical Society Reviews* **2015,** *44* (5), 1083-1100.
13. Bryliakov, K. P.; Talsi, E. P., Active sites and mechanisms of bioinspired oxidation with H2O2, catalyzed by non-heme Fe and related Mn complexes. *Coordination Chemistry Reviews* **2014,** *276*, 73-96.
14. Bryliakov, K. P., Catalytic Asymmetric Oxygenations with the Environmentally Benign Oxidants H2O2 and O2. *Chemical Reviews* **2017,** *117* (17), 11406-11459.
15. Vicens, L.; Costas, M., Biologically inspired oxidation catalysis using metallopeptides. *Dalton Transactions* **2018,** *47* (6), 1755-1763.
16. Krebs, C.; Galonić Fujimori, D.; Walsh, C. T.; Bollinger, J. M., Non-Heme Fe(IV)–Oxo Intermediates. *Accounts of Chemical Research* **2007,** *40* (7), 484-492.
17. Solomon, E. I.; Goudarzi, S.; Sutherlin, K. D., O2 Activation by Non-Heme Iron Enzymes. *Biochemistry* **2016,** *55* (46), 6363-6374.
18. Jasniewski, A. J.; Que, L., Dioxygen Activation by Nonheme Diiron Enzymes: Diverse Dioxygen Adducts, High-Valent Intermediates, and Related Model Complexes. *Chemical Reviews* **2018,** *118* (5), 2554-2592.
19. Castillo, R. G.; Banerjee, R.; Allpress, C. J.; Rohde, G. T.; Bill, E.; Que, L.; Lipscomb, J. D.; DeBeer, S., High-Energy-Resolution Fluorescence-Detected X-ray Absorption of the Q Intermediate of Soluble Methane Monooxygenase. *Journal of the American Chemical Society* **2017,** *139* (49), 18024-18033.
20. Cutsail, G. E.; Banerjee, R.; Zhou, A.; Que, L.; Lipscomb, J. D.; DeBeer, S., High-Resolution Extended X-ray Absorption Fine Structure Analysis Provides Evidence for a Longer Fe···Fe Distance in the Q Intermediate of Methane Monooxygenase. *Journal of the American Chemical Society* **2018,** *140* (48), 16807-16820.
21. Tinberg, C. E.; Lippard, S. J., Revisiting the Mechanism of Dioxygen Activation in Soluble Methane Monooxygenase from M. capsulatus (Bath): Evidence for a Multi-Step, Proton-Dependent Reaction Pathway. *Biochemistry* **2009,** *48* (51), 12145-12158.
22. Tinberg, C. E.; Lippard, S. J., Dioxygen Activation in Soluble Methane Monooxygenase. *Accounts of Chemical Research* **2011,** *44* (4), 280-288.
23. Gordon, J. B.; Vilbert, A. C.; DiMucci, I. M.; MacMillan, S. N.; Lancaster, K. M.; Moënne-Loccoz, P.; Goldberg, D. P., Activation of Dioxygen by a Mononuclear Nonheme Iron Complex: Sequential Peroxo, Oxo, and Hydroxo Intermediates. *Journal of the American Chemical Society* **2019,** *141* (44), 17533-17547.
24. Thibon, A.; England, J.; Martinho, M.; Young Jr., V. G.; Frisch, J. R.; Guillot, R.; Girerd, J.-J.; Münck, E.; Que Jr., L.; Banse, F., Proton- and Reductant-Assisted Dioxygen Activation by a Nonheme Iron(II) Complex to Form an Oxoiron(IV) Intermediate. *Angewandte Chemie International Edition* **2008,** *47* (37), 7064-7067.
25. Lee, Y.-M.; Bang, S.; Kim, Y. M.; Cho, J.; Hong, S.; Nomura, T.; Ogura, T.; Troeppner, O.; Ivanović-Burmazović, I.; Sarangi, R.; Fukuzumi, S.; Nam, W., A mononuclear nonheme iron(iii)–peroxo complex binding redox-inactive metal ions. *Chemical Science* **2013,** *4* (10), 3917-3923.
26. Li, F.; Van Heuvelen, K. M.; Meier, K. K.; Münck, E.; Que, L., Sc3+-Triggered Oxoiron(IV) Formation from O2 and its Non-Heme Iron(II) Precursor via a Sc3+–Peroxo–Fe3+ Intermediate. *Journal of the American Chemical Society* **2013,** *135* (28), 10198-10201.
27. Nishida, Y.; Lee, Y.-M.; Nam, W.; Fukuzumi, S., Autocatalytic Formation of an Iron(IV)–Oxo Complex via Scandium Ion-Promoted Radical Chain Autoxidation of an Iron(II) Complex with Dioxygen and Tetraphenylborate. *Journal of the American Chemical Society* **2014,** *136* (22), 8042-8049.
28. Engelmann, X.; Malik, D. D.; Corona, T.; Warm, K.; Farquhar, E. R.; Swart, M.; Nam, W.; Ray, K., Trapping of a Highly Reactive Oxoiron(IV) Complex in the Catalytic Epoxidation of Olefins by Hydrogen Peroxide. *Angewandte Chemie International Edition* **2019,** *58* (12), 4012-4016.
29. Hunter, T.; McNae, I.; Liang, X.; Bella, J.; Parsons, S.; Walkinshaw, M.; Sadler, P., Protein recognition of macrocycles: Binding of anti-HIV metallocyclams to lysozyme. *Proceedings of the National Academy of Sciences of the United States of America* **2005,** *102*, 2288-92.
30. Bosnich, B.; Poon, C. K.; Tobe, M. L., Complexes of Cobalt(III) with a Cyclic Tetradentate Secondary Amine. *Inorganic Chemistry* **1965,** *4* (8), 1102-1108.
31. Parish, R. V., *NMR, NQR, EPR, and Mossbauer spectroscopy in inorganic chemistry*. Ellis Horwood: Chichester, 1990.
32. 1H-NMR spectrum shows paramagnetically shifted signals in the range -30 – 165 ppm (Figure S6).
33. Que, J. L.; Puri, M., The Amazing High-Valent Nonheme Iron-Oxo Landscape. *Bulletin of Japan Society of Coordination Chemistry* **2016,** *67*, 10-18.
34. Cranswick, M. A.; Meier, K. K.; Shan, X.; Stubna, A.; Kaizer, J.; Mehn, M. P.; Münck, E.; Que, L., Protonation of a Peroxodiiron(III) Complex and Conversion to a Diiron(III/IV) Intermediate: Implications for Proton-Assisted O–O Bond Cleavage in Nonheme Diiron Enzymes. *Inorganic Chemistry* **2012,** *51* (19), 10417-10426.
35. Wang, D.; Ray, K.; Collins, M. J.; Farquhar, E. R.; Frisch, J. R.; Gómez, L.; Jackson, T. A.; Kerscher, M.; Waleska, A.; Comba, P.; Costas, M.; Que, L., Nonheme oxoiron(iv) complexes of pentadentate N5 ligands: spectroscopy, electrochemistry, and oxidative reactivity. *Chemical Science* **2013,** *4* (1), 282-291.
36. England, J.; Martinho, M.; Farquhar, E. R.; Frisch, J. R.; Bominaar, E. L.; Münck, E.; Que Jr., L., A Synthetic High-Spin Oxoiron(IV) Complex: Generation, Spectroscopic Characterization, and Reactivity. *Angewandte Chemie International Edition* **2009,** *48* (20), 3622-3626.
37. Chiang, C.-W.; Kleespies, S. T.; Stout, H. D.; Meier, K. K.; Li, P.-Y.; Bominaar, E. L.; Que, L.; Münck, E.; Lee, W.-Z., Characterization of a Paramagnetic Mononuclear Nonheme Iron-Superoxo Complex. *Journal of the American Chemical Society* **2014,** *136* (31), 10846-10849.
38. Musie, G. T.; Wei, M.; Subramaniam, B.; Busch, D. H., Autoxidation of Substituted Phenols Catalyzed by Cobalt Schiff Base Complexes in Supercritical Carbon Dioxide. *Inorganic Chemistry* **2001,** *40* (14), 3336-3341.
39. Company, A.; Yao, S.; Ray, K.; Driess, M., Dioxygenase-Like Reactivity of an Isolable Superoxo–Nickel(II) Complex. *Chemistry – A European Journal* **2010,** *16* (31), 9669-9675.

TOC Figure

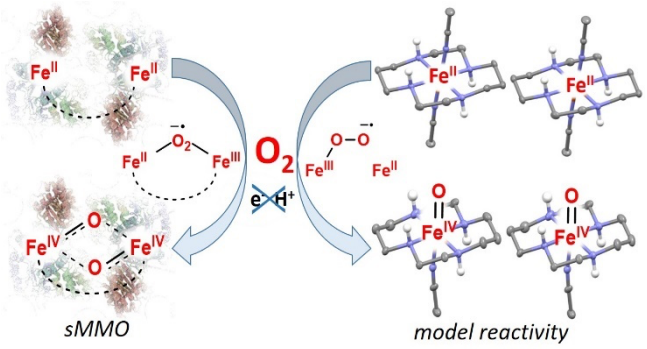
Fe^II
Fe^II
Fe^II
Fe^III
O2
Fe^IV
O
O
Fe^IV
sMMO
O2
e-
H+
O–O
Fe^III
Fe^II
Fe^II
Fe^II
O
Fe^IV
O
Fe^IV
model reactivity